Temperature and precipitation extremes in the United States: Quantifying the responses to anthropogenic aerosols and greenhouse gases

Nora R. Mascioli[1,2], Arlene M. Fiore[1,2], Michael Previdi[1], Gustavo Correa[1]

1. Department of Earth and Environmental Sciences, Columbia University, New York, New York, USA

2. Lamont-Doherty Earth Observatory of Columbia University, Palisades, New York, USA

Corresponding Author: Nora R. Mascioli

Address: 301F Oceanography

61 Route 9W – PO Box 1000

Palisades NY 10964-8000 US

Email: mascioli@ldeo.columbia.edu

Submitted to Journal of Climate July 2015

Abstract

Changes in extreme temperatures, heat waves, and heavy rainfall events have adverse effects on human health, air quality, and water resources. Using aerosol only (AER) and greenhouse gas only (GHG) simulations from the GFDL CM3 chemistry-climate model, we investigate aerosol- versus greenhouse gas-induced changes in temperature (summer) and precipitation (all seasons) extremes over the United States from 1860 to 2005. Small changes in these extremes in the "all forcing" simulations reflect cancellations between the effects of increasing anthropogenic aerosols and greenhouse gases. In AER, extreme high temperatures and the number of days with temperatures above the 90th percentile decline over most of the U.S. The strongest response occurs in the western U.S. (−2.0°C and −14 days, respectively, regionally averaged) and the weakest response occurs in the southeast (−0.6°C and −4.8 days). An opposite-signed response pattern occurs in GHG (+2.3°C and +11.5 days over the western U.S.; +1.6°C and +7.2 days over the southeast U.S.). The similar spatial response patterns in AER versus GHG suggest a preferred regional mode of response that is largely independent of the type of forcing. The weak response to forcing in the southeast U.S. is collocated with the observed "warming hole", a region where temperatures have declined during 1901-2012. Extreme precipitation over the eastern U.S. decreases in AER, particularly in winter, and increases over the eastern and central U.S. in GHG, particularly in spring. Over the 21st century under the RCP8.5 emissions scenario, the patterns of extreme temperature and precipitation associated with greenhouse gas forcing dominate.

1. Introduction

U.S. observations indicate increases over recent decades in extreme high temperatures, heat waves, and heavy rainfall events, with far reaching implications for human health, agriculture, air quality, water management, and economic growth (Kunkel et al. 2008). Heavy storms can incur property damage and threaten human life (Lott and Ross 2006), including through major flood events and flash floods (Kunkel et al. 2013). Summer heat waves have been shown to increase mortality by 2-5%; approximately 1000 deaths per year can be attributed to these events in the U.S. (Anderson and Bell 2011; Changnon et al. 1996), and extreme temperatures and heat waves correlate with extreme air pollution events (Logan et al. 1989; Tai et al. 2010; Tai et al. 2012; Leung et al. 2005; and others). Taken together, extreme heat and precipitation events cost the U.S. billions of dollars in damages each year (Lott and Ross 2006).

We use a state-of-the-art general circulation model (GCM) to investigate the historical changes in extreme temperature and precipitation in the United States in response to anthropogenic forcing. "Single forcing" GCM simulations allow us to individually assess the effects of anthropogenic aerosols (which typically cool the climate) and greenhouse gases (which warm the climate), revealing patterns of change not visible in the full historical simulations due to cross-cancellations. We find that aerosols have masked significant changes in high temperature and precipitation extremes that would otherwise have occurred in response to rising greenhouse gases. Global aerosol concentrations are projected to decrease over the 21st century due to air pollution controls; as a result, regional climate responses to greenhouse gases are expected to emerge.

Section 2 describes the model simulations and defines the extreme indices evaluated. In section 3, we discuss the modeled changes in U.S. extreme heat and precipitation as a result of increasing aerosols and greenhouse gases over the historical period (1860-2005). Section 4

projects future 21st century changes in extremes under the RCP8.5 scenario, in which greenhouse gas concentrations increase while aerosol emissions decrease. In Section 5, we discuss potential causes of the southeast U.S. "warming hole", and implications for future projections, and we conclude in Section 6.

2. Methods

2.1 Model description, simulations, and significance testing

We use the GFDL CM3 chemistry-climate model to evaluate changes in extreme temperature and precipitation over the United States induced by changes in aerosol and greenhouse gas burdens. CM3 simulations use a cubed sphere grid with 48 vertical levels; archived fields are regridded to a 2°× 2.5° latitude/longitude grid. In addition to its atmospheric component (AM3), CM3 includes the modular ocean model (MOM), a land component with dynamic vegetation (LM3), and a sea ice model, described in Donner et al. (2011). Of key importance for our study is the inclusion in AM3 of a more complex aerosol scheme that represents indirect effects of aerosols on clouds, as well as interactive tropospheric (and stratospheric) chemistry (Horowitz 2006; Ming et al. 2005; Ming et al. 2006; Naik et al. 2013). Aerosol concentrations are calculated from the ACCMIP historical (Lamarque et al. 2010) and RCP8.5 future (van Vuuren et al. 2011) emissions inventories, and undergo atmospheric transport, chemical transformations, and wet and dry deposition. AM3 accounts for anthropogenic and biomass burning emissions of aerosols and aerosol precursors, including sulfur dioxide, black carbon, and organic carbon (Lamarque et al. 2010); dimethyl sulfide emissions from sea water (Chin et al. 2002); dust (Ginoux et al. 2001); sea salt (Monahan et al. 1986); volcanic emissions of sulfur dioxide (Dentener et al. 2006); and a simple representation of

secondary organic aerosol production, including natural sources from plants and oceanic sea spray (Dentener et al. 2006; O'Dowd et al. 2008), as well as anthropogenic sources from the oxidation of butane (Tie et al. 2005).

In AM3, aerosols can interactively alter cloud properties by acting as cloud condensation nuclei. This impacts the size distribution of droplets in the cloud, producing clouds with smaller droplets, which reflect more incoming solar radiation (cloud albedo effect; Twomey 1977). In addition, smaller droplets are lighter and so less likely to precipitate out of the cloud, increasing its lifetime (cloud lifetime effect; Albrecht 1989). Both of these indirect effects of aerosols on clouds will tend to reduce incoming solar radiation, cooling the climate (Boucher et al. 2013). In the model, aerosol indirect effects occur only in liquid clouds; cloud droplet activation depends on the type of aerosol (sulfate, organic carbon and sea salt), its size distribution (which is assumed based on aerosol species), and updraft velocities within shallow cumulus and stratiform clouds (Donner et al. 2011, Golaz et al. 2013).

As part of the fifth Coupled Model Intercomparison Project (CMIP5), a number of simulations were designed to explore key regions of uncertainty in the climate system, for example forcing due to anthropogenic aerosols (Taylor et al. 2012). We use daily surface air temperature and precipitation data and monthly geopotential height, zonal and meridional wind, cloud fraction, surface shortwave flux, column water vapor, and soil moisture data from five of the simulations designed for CMIP5: the "aerosol only" simulations, with anthropogenic aerosols as the only time-varying forcing and all other forcings held at pre-Industrial levels (AER); "greenhouse gas only" simulations, with anthropogenic greenhouse gases as the only time-varying forcing (GHG); the full historical simulations (HIST), with all natural and anthropogenic forcings (including land-use changes) varying in time; a future emissions scenario, RCP8.5, in

which greenhouse gases increase from 2006 through 2100, while anthropogenic aerosols decrease (Riahi et al. 2011); and an 800-year pre-Industrial control run. Additionally, we analyze a modified future scenario in which greenhouse gases follow their trajectory from RCP8.5, while aerosol concentrations are held constant at 2005 levels (RCP8.5_2005Aer; Westervelt et al. 2015). The AER, GHG, RCP8.5, and RCP8.5_2005Aer simulations each consist of three ensemble members, differing only in their initial conditions; the historical simulation has five ensemble members; and the pre-Industrial control run consists of a single ensemble member. The AER, GHG, and historical simulations are run from 1860 through 2005.

We consider the ensemble mean changes in each CM3 simulation. The statistical significance of these changes is assessed using two methods. In the first method, we use a z-test to determine where the difference between 30-year means is statistically different from zero (95% confidence). In the second method, the 800-year control run is split into distinct 30-year segments. We then construct a probability density function for the difference between the means of two randomly selected 30-year segments. Differences in the forced simulations that fall outside the 95% confidence interval of this distribution are considered to be outside the range of natural variability.

2.2 Extreme Indices

The extreme climate indices defined by the Expert Team on Climate Change Detection and Indices (ETCCDI; Sillmann et al. 2013a,b) serve as the basis for our analysis, with a focus on two temperature indices (TXx, TX90p) and two precipitation indices (PRCPTOT, R99p). TXx is the maximum of the maximum daily temperature over a given time period. TX90p represents the number of days with a maximum temperature above the 90^{th} percentile (defined

using a moving 5 day window computed over a 30 year base period). PRCPTOT is the total precipitation over a given time period. R99p, representing extreme precipitation, is the total amount of precipitation occurring on days with precipitation values above the 99th percentile of the climatology. For the two threshold based indices, TX90p and R99p, 1961-1990 is used as the climatological base period. Further details on these indices are provided in Sillmann et al. (2013a,b).

2.3 Model evaluation

CM3 captures the observed global climatology from 1981-2000 in the two metrics for extreme temperature considered in this work. Compared with the ERA40, ERA-Interim, NCEP1 and NCEP2 reanalyses, CM3 performs well, relative to the suite of CMIP5 models (Sillmann et al. 2013a). With regards to the mean temperature, CM3 has a known summertime cold bias of −2.24°C, evenly distributed over the U.S.A. with respect to temperature observations from CRU from 1979-2005 (Donner et al. 2011; Sheffield et al. 2013). Despite the bias, the model captures the spatial distribution of observed summertime temperatures. The summer cold bias is likely due to a "cloud lifetime effect" (aerosol second indirect effect) that is too strong in the model (Ackerman et al. 2004; Quaas et al. 2009; Guo et al. 2011; Golaz et al. 2013; Levy et al. 2013). Modeled winter temperatures are in good agreement with observations from CRU, with a mean bias of only −0.03°C over the continental U.S. (Sheffield et al. 2013).

CM3 also does well relative to the suite of CMIP5 models at capturing the annual global climatology of extreme precipitation (R99p) from 1981-2000 calculated from the four sets of reanalysis data (Sillmann et al. 2013a). CM3 has excessive seasonal mean precipitation over much of North America in winter in comparison to the 1979-2005 climatology from GPCP

(Sheffield et al. 2013), most pronounced over western North America (+52.7% of the observed mean), and much smaller over eastern North America (+4.46% of observed mean). Sheffield et al. (2013) also find a small low bias in mean precipitation over central North America in winter (−2.6% of the observed mean). Despite these biases, CM3 generally captures the observed spatial distribution of wintertime precipitation (Sheffield et al. 2013). In summer, CM3 has relatively small biases in mean precipitation over eastern and central North America (−4.38% and +7.45% of the observed mean, respectively), and a high bias over western North America (+54.74% of the observed mean). The model does not capture the observed spatial distribution of summertime precipitation over the U.S.A., a common weakness amongst CMIP5 models, most likely due to a failure to properly represent the dynamical conditions that produce summertime precipitation (Sheffield et al. 2013; G. Vecchi, personal communication, April 10, 2015).

3. Historical changes over the U.S.A.: Greenhouse gases vs. aerosols

3.1 Temperature extremes

In this section we examine summertime changes in TX90p and TXx, which provide information on changes in the magnitude and frequency of extreme high temperatures, using the AER, GHG, and HIST simulations (Section 2.1). Significant changes in summertime TX90p occur in AER and GHG over this time period (Fig. 1a,b). Aerosols generally lead to decreases in TX90p while greenhouse gases generally lead to increases. Increasing greenhouse gases produce warming outside of the range of natural variability everywhere in the U.S., while increasing aerosols produce cooling outside of the range of natural variability over most of the U.S., with the exception of the southeast U.S. (discussed further in Section 5). Changes in the historical

simulations, from 1860-2005, are generally not statistically significantly outside the range of natural variability as determined by the pre-Industrial control simulation (Fig. 1c).

Greenhouse gases (with the exception of ozone) are long-lived and thus well mixed in the atmosphere, while aerosols have a heterogeneous spatial distribution. However, Fig. 1a,b shows a statistically significant anti-correlation between the response patterns associated with greenhouse gases and aerosols over the U.S., with a pattern correlation coefficient of −0.72. In both AER and GHG the largest temperature changes occur in the western U.S. (−14.0 and +11.5 days respectively), with relatively weaker changes in the northeast U.S. (−9.6 and +10.9 days), and little to no statistically significant change in the southeast U.S. (−4.8 and +7.2 days). This response pattern is consistent with observations showing a relative intensification of warming in the western U.S. in comparison with the eastern U.S. over the 20th century (Meehl et al. 2012; Donat et al. 2013). Due to the similarity in spatial response pattern and magnitude between GHG and AER, there is a cancellation between these two competing effects in the "all forcing" simulation, resulting in little to no change in TX90p in Fig. 1c.

TXx similarly shows a significant anti-correlation between the effects of greenhouse gases and aerosols, with a pattern correlation coefficient of –0.64 (Fig. 1d,e). The largest responses to anthropogenic forcing occur in the western U.S., where aerosols reduce TXx by –2.0°C and greenhouse gases increase TXx by 2.3°C. The response in the southeast U.S. is relatively weak, with aerosols reducing TXx by −0.6°C and greenhouse gases increasing TXx by 1.6°C. As for TX90p, cancellations between the effects of aerosols and greenhouse gases on TXx result in relatively small changes in the historical simulation (Fig. 1f).

3.2 Precipitation extremes

Overall, aerosols tend to reduce precipitation in the U.S. while greenhouse gases tend to increase it (Fig. 2, Supplemental Fig. 1). However, the spatial distribution of changes in precipitation varies in some seasons in response to different types of forcing. This finding is consistent with previous modeling studies that found that the precipitation response pattern is dependent on the type of forcing agent and its spatial distribution (e.g. Kloster et al. 2009; Shindell et al. 2012). Wintertime extreme precipitation in the eastern U.S. increases significantly in GHG (18 mm in the southeast and 7.2 mm in the northeast) and decreases significantly in AER (−14 mm in the southeast and −4.5 mm in the northeast), with a correlation coefficient of −0.62 (Fig. 2a,b). Changes elsewhere in the U.S.A. are not significant in winter. In the spring, extreme precipitation in AER decreases slightly in the eastern U.S., but it is not significant (Fig. 2d). However, in GHG, springtime extreme precipitation increases over most of the central and eastern U.S.A (Fig. 2e). In this season, the correlation coefficient between AER and GHG is only −0.24, suggesting that different mechanisms determine the springtime impacts of aerosols and greenhouse gases on extreme precipitation. Changes in HIST are shown for both seasons for completeness, but are not significant (Fig. 2c,f). Changes in extreme precipitation in summer and fall are less significant than those in winter and spring and are shown in Supplemental Fig. 2.

4. Future changes in U.S. temperature and precipitation extremes

4.1 Extreme temperatures become the new normal

Under the RCP8.5 scenario, in which anthropogenic radiative forcing reaches approximately 8.5 W m^{-2} by 2100 (relative to the pre-Industrial), the well-mixed greenhouse gases increase steadily throughout the 21st century, while emissions of short-lived pollutants (aerosols, and aerosol and tropospheric ozone precursors) decrease dramatically due to air

quality regulations (Riahi et al. 2011). By mid-century, the warming signal associated with the combined effects of increasing greenhouse gas concentrations and decreasing aerosol concentrations is clearly apparent over the U.S., with increases in TX90p on the order of 40 to 50 days per summer (Fig. 3a,b), and increases in TXx between 2.5 to 6.0°C (Fig. 3c,d). By the end of the century, TX90p saturates with respect to the 1961-1990 climatology and almost all summer days lie above the 90th percentile thresholds. By the end of the 21st century, TXx has increased substantially by 5 to 10°C across the U.S. For both TX90p and TXx, the spatial pattern of the temperature response in the 21st century is similar to the GHG simulation (Fig. 1b,e; Supplemental Figs. 3 and 4). Although significant warming occurs everywhere by mid-century, the southeast U.S. warms less rapidly than the rest of the country. This feature is discussed in Section 5.

We investigate next how long it will take before future anthropogenic climate change can be expected to exceed the range of natural variability (which does not occur in HIST due to cancellation between aerosols and greenhouse gases). We define the time of emergence as the first year when the difference between the 30-year mean centered on that year and the end of the twentieth century (1975-2005) is outside of the range of natural variability in the pre-Industrial control simulation (following the approach described above). For both TX90p and TXx, the climate change signal becomes detectable within the first few decades of the 21st century, over most of the U.S (Fig. 4a,b).

In order to separate the effects of decreasing aerosol concentrations and increasing greenhouse gas concentrations, we examine a second future scenario, RCP8.5_2005Aer, in which greenhouse gas concentrations follow their RCP8.5 trajectory while aerosols are held constant at 2005 levels. The dashed lines in Fig. 3 show that holding aerosols constant reduces

future increases in TX90p and TXx relative to RCP8.5. By mid-century, TX90p is reduced by an average of 15 days per summer in the eastern U.S., and by an average of 10 days per summer in the central and western U.S. By the end of the 21st century, TX90p is reduced by an average of 10 days per summer over the continental U.S., although even with aerosols held constant at 2005 levels, the index is approaching saturation. Similarly, the continued presence of aerosols at 2005 levels reduces mid-century increases in TXx by 1.5°C over the eastern U.S., and 1.0°C over the central and western U.S. By the end of the century increases in TXx are reduced by 1.5°C in the southeast U.S., and 1.75°C in the rest of the U.S. on average.

Even with aerosols held constant at 2005 levels, statistically significant increases in extreme temperatures still occur due to rising greenhouse gases over the entire U.S. By mid-century, TX90p has increased by 25 to 35 days per summer across most of the U.S., and by the end of the century, it has increased by 55 to 65 days per summer, indicating that more than two thirds of the summer days are above the 1961-1990 90th percentile threshold. TXx increases by 2.5 to 3.5°C by mid-century, and by 5 to 6°C by the end of century, reflecting the dominant influence of greenhouse gases. For both indices, the time of emergence (Fig. 4c,d) is delayed by at most 5 years over most of the U.S. when aerosols are maintained at 2005 levels.

4.2 Extreme precipitation: shifting towards a wetter future

Future changes in extreme precipitation also show patterns associated with the greenhouse gas signal evident from the 1860-2005 GHG simulation. By the end of the 21st century, wintertime R99p has increased significantly over the eastern and northwest U.S. (Supplemental Fig. 5). In the southeast and northeast U.S., R99p increases by 32 mm and 42 mm respectively (Fig. 5a), while it increases in the western U.S. by 18 mm (Fig. 5b). In spring,

R99p increases significantly over the eastern and north-central U.S. (Supplemental Fig. 5). By the end of the 21st century, springtime R99p has increased by 30 mm in the southeast U.S., and by 40 mm in the northeast U.S. (Fig. 5c). On average, comparing 2070-2100 to 1975-2005, springtime R99p increases by 9.5 mm in the central U.S. (Fig. 5d), but with a region in the north-central U.S. that increases by 30 mm (Supplemental Fig. 5d). Summertime changes in extreme precipitation are generally not significant (Supplemental Fig. 5). Finally, in fall, there are statistically significant increases in R99p in the northeast and northwest, averaging 25 and 15 mm by end of century respectively (Fig. 5e,f; Supplemental Fig. 5). This is particularly noteworthy because, in contrast with winter and spring, there are generally no statistically significant changes in total precipitation in this season (Supplemental Fig. 6). This indicates a change in the shape of the overall distribution of precipitation, with a tendency towards more extreme precipitation.

The climate change signal is slower to emerge for precipitation than for temperature. The changes emerge as significant early in the 21st century in the eastern U.S. in winter and spring (Fig. 6a,b); in the western U.S. in winter, the signal emerges by 2050; and in autumn, the signal emerges late in the 21st century in the Midwest and pacific northwest (Supplemental Fig. 7b). The impacts of reductions in aerosol concentrations on extreme precipitation are minimal over the 21st century (Fig. 5), and changes in the time of emergence are small (Fig. 6, Supplemental Fig. 7).

5. Southeast U.S. "warming hole"

The absence of statistically significant cooling in the southeast U.S. in the AER simulations (Fig. 1a,d) and weak warming in the GHG simulations (Fig. 1b,e) is of particular

note due to observations of a "warming hole" in this region over the 20th century (Donat et al. 2013; Meehl et al. 2012; and others). Previous research indicates the summertime warming hole is likely connected to changes in the hydrological cycle driven by changes in the regional circulation patterns (Pan et al. 2004; Portmann et al. 2009; Leibensperger et al. 2012; Weaver et al. 2012; Meehl et al. 2012; Yu et al. 2014). Whether or not these changes are due to natural variability, associated with relative changes in Pacific and Atlantic sea surface temperatures (SSTs; Meehl et al. 2012; Weaver et al. 2012), or anthropogenic forcing due to aerosols (Leibensperger et al. 2012; Yu et al. 2014) and land use change (Misra et al. 2012), is still debated.

In keeping with previous studies, the weak temperature response in the southeast U.S. in CM3 is due to changes in the hydrological cycle in the region affecting the surface energy budget. During summer, aerosols decrease total precipitation in the southeast U.S., while greenhouse gases increase it (Supplemental Fig. 1g,h). In AER, this precipitation decrease is consistent with a reduction in moisture transport into the region, and an accompanying reduction in the total cloud fraction (Fig. 7b,c). Total column water vapor (not shown) also decreases in the region. This produces the two-fold effect of reducing the soil moisture content (Fig. 7a), which contributes to increased sensible versus latent heating of the near-surface air, and increasing the shortwave (SW) radiation absorption at the surface (Fig. 7d). Both of these processes act to produce the muted temperature response over the southeast U.S. in AER.

Previous studies have shown that changes in the westward extent of the Bermuda High are critical for determining the position of the Great Plains low-level jet, and thus the amount of summertime precipitation in the southeast U.S. (Li et al. 2011; Zhu and Liang 2013). In AER, we find that the Bermuda High is weakened along its westward edge, weakening the 850 hPa

winds blowing moisture-laden air from the Gulf of Mexico into the southeast U.S., and contributing to the changes in the hydrology discussed above (Fig. 7e,f). This result contrasts with earlier findings using the GISS model, in which U.S. aerosols strengthened the Bermuda High, driving a circulation which increased the moisture transport into the southeast U.S., and produced a strong cooling trend in the region (Leibensperger et al. 2012).

In GHG, the regional increases in precipitation are accompanied by increases in the moisture flux into the southeast U.S. and decreases in the SW absorption at the surface (Fig. 8b,d). Increases in total column water vapor (not shown) contribute to the decreases in SW absorption at the surface. The total cloud fraction does not change significantly over the southeast U.S.; however, large-scale decreases in total cloud fraction occur over the rest of the eastern and central U.S., which likely contribute to enhanced warming outside of the southeast (Fig. 8c). Changes in soil moisture content do not contribute to the weak warming in the southeast U.S. in GHG (Fig. 8a). Although the Bermuda High is strengthened, we do not find clear evidence of low-level circulation changes to explain the change in the transport of moisture into the southeast U.S. (Fig. 8e,f). Therefore, further analysis is required to determine the mechanisms driving the changes in the hydrological cycle over the southeast U.S. in response to rising greenhouse gases.

6. Conclusions

The ETCCDI extreme climate indices have been used as a metric for investigating changes in extreme temperature and precipitation in the U.S. As expected, high temperature extremes in the U.S. generally decrease in response to aerosols and increase in response to greenhouse gases. We identify clear regional patterns of response to forcing: the western U.S.

has the strongest response to both aerosols and greenhouse gases, while the weakest response occurs in the southeast U.S. (Fig. 1). This compares well with observations of temperature trends in the U.S., and gives us confidence in the model representation of spatial patterns of temperature extremes (Meehl et al. 2012; Sheffield et al. 2013).

Overall, simulated precipitation changes during the historical period are concentrated in the eastern and central U.S., the regions where the model best captures the observed patterns (Sheffield et al. 2013). In the CM3 model, aerosols tend to reduce extreme precipitation, while greenhouse gases tend to increase it, particularly in the spring (Fig. 2). Although changes in the historical simulation are not significantly different from zero, we note that in the GHG simulation there are large increases in R99p in the Midwest, particularly in spring. This coincides with observed statistically significant increases in extreme precipitation in the Midwest in spring, suggesting the observed trend may be due to greenhouse gases (Kunkel et al. 2008).

The signal associated with greenhouse gases emerges clearly by the end of the 21st century for all indices in the extreme warming scenario, RCP8.5. As a result of the combined effects of increasing greenhouse gas concentrations and decreasing aerosol emissions (but primarily the former), by the end of the century, the entire summer lies above the 90th percentile of daily maximum temperature from 1961-1990. Seasonal extreme precipitation in winter and spring in the northeast and central U.S. increases by up to 40 mm. In fall, extreme precipitation increases in the northeast and northwest U.S. despite a lack of significant changes in total precipitation, indicating a change in the shape of the precipitation distribution. Total summertime precipitation increases in the southeast U.S., although there are no significant changes in extreme precipitation.

The lack of statistically significant cooling in the southeast U.S. in the aerosol only simulations and collocated warming minimum in the greenhouse gas only simulations are of particular interest because of the observed warming hole in this region (e.g. Hartmann et al. 2013; Meehl et al. 2012; Leibensperger et al. 2012; Donat et al. 2013). Previous studies focusing on the warming hole have identified several potential natural and anthropogenic causes of this feature, such as changes in local hydroclimate, changes in SST forcing from the Pacific and Atlantic, and cooling as a result of aerosol forcing. In the GFDL CM3 model, the persistence of this feature over multiple decades, across multiple ensemble members and different forcing scenarios, suggests that it is a characteristic response to radiative forcing in this model. This response is consistent with changes in local hydroclimate: changes in soil moisture content in AER and total cloud fraction in both AER and GHG affect the surface energy budget by changing the partitioning of sensible and latent heating and the surface absorption of shortwave radiation.

Extreme events have major impacts on human health and economics. In order to predict future changes in these damaging events, we need to improve our understanding of how extreme temperature and precipitation respond to different types of anthropogenic forcing. In the GFDL CM3 model, there are no statistically significant changes in these extremes in the full historical simulation during 1860-2005. However, using single-forcing simulations for the same time period, we find that anthropogenic aerosols and greenhouse gases individually have significant impacts on extremes. In general, it is the cancellation between the effects of aerosols and greenhouse gases that results in the absence of statistically significant changes in the historical simulations. In the future, as aerosol emissions decrease and greenhouse gas concentrations

continue to increase, the impacts of anthropogenic climate change on extreme weather in the U.S. will emerge.

Acknowledgments

This article was made possible by EPA-STAR grant 83520601. Its contents are solely the responsibility of the grantee and do not necessarily represent the official view of the EPA. Further, the EPA does not endorse the purchase of any commercial products or services mentioned in the publication.

References

Ackerman, A. S., M. P. Kirkpatrick, D. E. Stevens, and O. B. Toon, 2004: The impact of humidity above stratiform clouds on indirect aerosol climate forcing. *Nature*, **432**, 1014–1017, doi:10.1038/nature03174.

Albrecht, B.A., 1989: Aerosols, cloud microphysics, and fractional cloudiness. *Science*, **245**, 1227-1230, doi:10.1126/science.245.4923.1227.

Anderson, G. B., and M. L. Bell, 2011: Heat Waves in the United States: mortality risk during heat waves and effect modification by heat wave characteristics in 43 U.S. communities. *Environ. Health Perspect.,* **119**, 210-218, doi:10.1289/ehp.1002313.

Boucher, O. and Coauthors, 2013: Clouds and aerosols. In *Climate Change 2013: The Physical Science Basis. Contribution of Working Group I to the Fifth Assessment Report of the Intergovernmental Panel on Climate Change*. T.F. Stocker, D. Qin, G.-K. Plattner, M. Tignor, S.K. Allen, J. Doschung, A. Nauels, Y. Xia, V. Bex, and P.M. Midgley, Eds. Cambridge University Press, 571-657, doi:10.1017/CBO9781107415324.016.

Changnon, S. A., K. E. Kunkel, and B. C. Reinke, 1996: Impacts and response to the 1995 heat wave: a call to action. *Bull. of the Amer. Met. Soc.,* **77**, 1497-1506, doi: http://dx.doi.org/10.1175/1520-0477(1996)077<1497:IARTTH>2.0.CO;2.

Chin, M., and Coauthors, 2002: Tropospheric aerosol optical thick- ness from the GOCART model and comparisons with satellite and sun photometer measurements. *J. Atmos. Sci.*, **59**, 461–483, doi: http://dx.doi.org/10.1175/1520-0469(2002)059<0461:TAOTFT>2.0.CO;2.

Dentener, F., and Coauthors, 2006: Emissions of primary aerosol and precursor gases in the years 2000 and 1750 prescribed data-sets for AeroCom. *Atmos. Chem. Phys.*, **6**, 4321–4344, doi:10.5194/acp-6-4321-2006.

Donat, M. G. and Coauthors, 2013: Updated analyses of temperature and precipitation extreme indices since the beginning of the twentieth century: the HadEX2 dataset. *J. of Geophys. Res.*, **118**, 1-16, doi:10.1002/jgrd.50150.

Donner, L. J. and Coauthors, 2011: The dynamical core, physical parameterizations, and basic simulation characteristics of the atmospheric component AM3 of the GFDL global coupled model CM3. *J. Clim.*, **24**, 3484-3519, doi:10.1175/2011JCLI3955.1.

Ginoux, P., M. Chin, I. Tegen, J. M. Prospero, B. Holben, O. Dubovik, and S.-J. Lin, 2001: Sources and distributions of dust aerosols simulated with the GOCART model. *J. Geophys. Res.*, **106**, 22 255–22 274, doi:10.1029/2000JD000053.

Golaz, J.-C., L. W. Horowitz, and H. Levy II, 2013: Cloud tuning in a coupled climate model: Impact on 20th century warming. *Geophys. Res. Lett.*, **40**, 2246–2251, doi:10.1002/grl.50232.

Guo, H., J.-C. Golaz, and L. J. Donner, 2011: Aerosol effects on stratocumulus water paths in a PDF-based parameterization. *Geophys. Res. Lett.*, **38**, L17808, doi:10.1029/2011GL048611.

Hartmann, D.L. and Coauthors, 2013: Observations: Atmosphere and Surface. In *Climate Change 2013: The Physical Science Basis. Contribution of Working Group I to the Fifth Assessment Report of the Intergovernmental Panel on Climate Change*. T.F. Stocker, D. Qin, G.-K. Plattner, M. Tignor, S.K. Allen, J. Doschung, A. Nauels, Y. Xia, V. Bex, and P.M. Midgley, Eds. Cambridge University Press, 571-657, doi:10.1017/CBO9781107415324.016.

Horowitz, L.W., 2006: Past, present, and future concentrations of tropospheric ozone and aerosols: Methodology, ozone evaluation, and sensitivity to aerosol wet removal. *J. Geophys. Res.*, **111**, D22211, doi:10.1029/2005JD006937.

Kloster, S., F. Dentener, J. Feichter, F. Raes, E. Roeckner, U. Lohmann, I. Fischer-Bruns, 2009: A GCM study of future climate response to air pollution reduction. *Clim. Dyn.*, **34**, 1177-1194, doi: 10.1007/s0038-009-0537-0.

Kunkel, K. E. and Coauthors, 2008: Observed changes in weather and climate extremes. *Weather and Climate Extremes in a Changing Climate. Regions of Focus: North America, Hawaii, Caribbean, and U.S. Pacific Islands*. Karl, T. R., G. A. Meehl, C. D. Miller, S. J. Hassol, A. M. Waple, and W. L. Murray, Eds., UNT Digital Library, 35-79.

Kunkel, K. E. and Coauthors, 2013: Monitoring and understanding trends in extreme storms: State of knowledge. *Bulletin of the Amer. Met. Soc.*, **94**, 499-514, doi:10.1175/BAMS-D-11-00262.1.

Lamarque, J.-F., and Coauthors, 2010: Historical (1850–2000) gridded anthropogenic and biomass burning emissions of re- active gases and aerosols: Methodology and application. *Atmos. Chem. Phys.*, **10**, 7017-7039, doi:10.5194/acp-10-7017-2010.

Leibensperger, E. M., L. J. Mickley, D. J. Jacob, W.-T. Chen, J. H. Seinfeld, A. Nenes, P. J. Adams, D. G. Streets, N. Kumar, D. and Rind, 2012: Climatic effects of 1950-2050 changes in US anthropogenic aerosols – Part 2: Climate response. *Atmos. Chem. Phys.,* **12**, 3349-3362, doi:10.5194/acp-12-3349-2012.

Leung, R. L., W. I. Gustafson Jr., 2005: Potential regional climate change and implications to US air quality. *Geophys. Res. Lett.*, **32**, L16711, doi:10.1029/2005GL022911.

Levy II, H., L. W. Horowitz, M. D. Schwarzkopf, Y. Ming, J.-C. Golaz, V. Naik, V. and Ramaswamy, 2013: The roles of aerosol direct and indirect effects in past and future climate change. *J. Geophys. Res.*, **118**, 1-12, doi:10.1002/jgrd.50192.

Li, L., W. Li, and Y. Kushnir, 2012: Variation of North Atlantic Subtropical High western ridge and its implication to the Southeastern US summer precipitation. *Clim. Dyn.*, **45**, 67-82, doi: 10.1007/s00382-014-2216-3.

Logan, J. A., 1989: Ozone in rural areas of the United States. *J. Geophys. Res.*, **94**, 8511-8532, doi: 10.1029/JD094iD06p08511.

Lott, N. and T. Ross, 2006: Tracking and evaluating U.S. billion dollar weather disasters, 1980-2005. *86th AMS annual meeting,* Atlanta, GA, Amer. Meteor. Soc., 1.2. [available online at http://ams.confex.com/ams/pdfpapers/100686.pdf].

Meehl, G., J. Arblaster, and G. Branstator, 2012: Mechanisms contributing to the warming hole and the consequent U.S. east-west differential of heat extremes. *J. Climate*, **25**, 6394-6408 doi:0.1175/JCLI-D-11-00655.1.

Ming, Y., V. Ramaswamy, L. Donner, V. T. J. Phillips, 2005: A new parameterization of cloud droplet activation applicable to general circulation models. *J. of Atmos. Sci.,* **63**, 1348, doi:http://dx.doi.org/10.1175/JAS3686.1.

Ming, Y., V. Ramaswamy, L. Donner, V. T. J. Phillips, S. A. Klein, P. A. Ginoux, L. W. Horowitz, 2006: Modeling the interactions between aerosols and liquid water clouds with a self-consistent cloud scheme in a general circulation model. *J. Atmos. Sci.,* **64**, 1189-1209, doi:http://dx.doi.org/10.1175/JAS3874.1.

Misra, V., J.-P. Michael, R. Boyles, E. P. Chassignet, M. Griffin, and J. J. O'Brien, 2012: Reconciling the Spatial Distribution of the Surface Temperature Trends in the Southeastern United States. *J. Climate*, **25**, 3610–3618. doi: http://dx.doi.org/10.1175/JCLI-D-11-00170.1.

Monahan, E. C., D. E. Spiel, and K. L. Davidson, 1986: A model of marine aerosol generation via whitecaps and wave disruption. *Oceanic Whitecaps*, E. C. Monahan and G. Mac Niocaill, Eds., D. Reidel, 167–174.

Naik, V., L. W. Horowitz, A. M. Fiore, P. Ginoux, J. Mao, A. M. Aghedo, and H. Levy II, 2013: Impact of preindustrial to present-day changes in short-lived pollutant emissions on atmospheric composition and climate forcing. *J. Geophys. Res.,* **118**, 8086-8110, doi:10.1002/jgrd.50608.

O'Dowd, C.D., B. Langmann, S. Varghese, C. Scannell, D. Ceburnis, and M. C. Facchini, 2008: A combined organic-inorganic seaspray source function. *Geophys. Res. Lett.*, **35**, L01801, doi:10.1029/2007GL030331.

Pan, Z., R. W. Arritt, E. S. Takle, W. J. Gutowski Jr., C. J. Anderson, and M. Segal., 2004: Altered hydrologic feedback in a warming climate introduces a "warming hole". *Geophys. Res. Lett.,* **31**, L17109, doi:10.1029/2004GL020528.

Portmann, R. W., S, Solomon, and G. C. Hegerl, 2009: Spatial and seasonal patterns in climate change, temperatures, and precipitation across the United States. *Proc. Natl. Acad. Sci. USA* **106**, 7324–7329 doi: 10.1073/pnas.0808533106.

Quaas, J., and Coauthors, 2009: Aerosol indirect effects — General circulation model intercomparison and evaluation with satellite data. *Atmos. Chem. Phys.*, **9**, 8697–8717, doi:10.5194/acp-9-8697-2009.

Riahi, K., S. Rao, V. Krey, C. Cho., V. Chirkov, G. Fischer, G. Kindermann, N. Nakicenovic and P. Rafaj, 2011: A scenario of comparatively high greenhouse gas emissions. *Climatic Change*, **109**, 33-57, doi:10.1007/s10584-011-0149.

Sheffield, J. and Coauthors, 2013: North American Climate in CMIP5 Experiments. Part I: Evaluation of Historical Simulations of Continental and Regional Climatology. *J. Climate*, **26**, 9209–9245, doi: http://dx.doi.org/10.1175/JCLI-D-12-00592.1.

Shindell, D. T., A. Voulgarakis, G. Faluvegi, G. Milly, 2012: Precipitation response to regional radiative forcing. *Atmos. Chem. Phys.*, **12**, 6969-6982, doi:10.5194/acp-12-6969-2012.

Sillmann, J., V. V. Kharin, X. Zhang, F. W. Zwiers, and D. Bronaugh, 2013a: Climate extremes indices in the CMIP5 multimodel ensemble: Part1. Model evaluation in the present climate. *J. Geophys. Res.*, **118**, 1716-1733, doi:10.1002/jgrd.50203.

Sillmann, J., V. V. Kharin, F. W. Zwiers, X. Zhang, and D. Bronaugh, 2013b: Climate extremes indices in the CMIP5 multimodel ensemble: Part2. Future climate projections. *J. Geophys. Res.*, **118**,2473-2493, doi:10.1002/jgrd.50188.

Tai, A. P. K., L. J. Mickley, D. J. Jacob, E. M. Leibensperger, L. Zhang, J. A. Fisher, and H. O. T. Pye, 2012: Meteorological modes of variability for fine particulate matter ($PM_{2.5}$) air quality in the United States: implications for $PM_{2.5}$ sensitivity to climate change. *Atmos. Chem. Phys.*, **12**, 3131-3145, doi:10.5194/acp-12-3131-2012.

Tai, A. P. K., L. J. Mickley, D. J. Jacob, 2010: Correlations between fine particulate matter (PM 2.5) and meteorological variables in the United States: Implications for the sensitivity of PM2.5 to climate change. *Atmos. Environ.,* **44**, 3976-3984, doi:10.1016/j.atmosenv.2010.06.060.

Taylor, K.E., R. J. Stouffer, G. A. Meehl, 2012: An overview of CMIP5 and the experiment design. *Bull. Amer. Meteor. Soc.*, **93**, 485-498, doi:10.1175/BAMS-D-11-00094.1.

Tie, X., and Coauthors, 2005: Assessment of the global impact of aerosols on tropospheric oxidants. *J. Geophys. Res.*, **110**, D03204, doi:10.1029/2004JD005359.

Twomey, S., 1977: The influence of pollution on the shortwave albedo of clouds. *J. Atmos. Sci.*, **34**, 1149–1152.

Weaver, S., 2012: Factors associated with decadal variability in Great Plains summertime surface temperatures. *J. Climate,* **26**, 343-349, doi:10.1175/JCLI-D-11-00713.1.

Westervelt D. M., L. W. Horowitz, V. Naik, and D. L. Mauzerall, 2015: Radiative forcing and climate response to projected 21st century aerosol decreases. *Atmos. Chem. Phys. Disc.*, **15**, 9293-9353, doi:10.5194/acpd-15-9293-2015.

Yu, S., K. Alapaty, R. Mathur, J. Pleim, Y. Zhang, C. Nolte, B. Eder, K. Foley, and T. Nagashima, 2014: Attribution of the United States "warming hole": Aerosol indirect effect and precipitable water vapor. *Sci. Rep.*, **4**, 1-10, doi:10.1038/srep06929.

Zhu, J. and X.-Z. Liang, 2013: Impacts of the Bermuda High on Regional Climate and Ozone over the United States. *J. Climate*, **26**, 1018–1032, doi: http://dx.doi.org/10.1175/JCLI-D-12-00168.1.

Figure Captions

Figure 1. Changes in the 30-year ensemble mean values of summer (JJA) TX90p (top) and TXx (bottom) between the beginning (1860-1890) and end (1976-2006) of the aerosol-only (a), greenhouse gas only (b), and historical simulations (c). Xs denote that the changes are outside of the range of natural variability (95% confidence), as determined from the model's pre-Industrial control simulation.

Figure 2. Changes in the 30-year ensemble mean values of R99p between the beginning (1860-1890) and end (1976-2006) of the aerosol only (left), greenhouse gas only (middle) and historical (right) scenarios in winter (top) and spring (bottom).

Figure 3. Summertime TX90p (top) and TXx (bottom) for RCP8.5 (solid) and RCP8.5_2005Aer(dashed) for different regions in the U.S., expressed as anomalies with respect to 1975-2005. The tapering off in TX90p at the end of the 21st century is an artifact of the index becoming saturated with respect to the 1961-1990 thresholds.

Figure 4. Time of emergence for changes in 30-yr mean TX90p (a)(c) and TXx (b)(d) relative to the present day (1975-2005) for the RCP8.5 scenario (top) and RCP8.5 with aerosols held constant at 2005 levels (bottom). Colors indicate the midpoint of the earliest 30-yr period for which the difference is outside the range of natural variability relative to the pre-Industrial control run.

Figure 5. Winter (top), spring (middle), and fall (bottom) R99p for RCP8.5 (solid) and RCP8.5_2005Aer(dashed) for different regions in the U.S., expressed as anomalies with respect to 1975-2005.

Figure 6. Time of emergence for changes in 30-yr mean R99p for winter (left) and spring (right) relative to the present day (1975-2005) for the RCP8.5 (top) and RCP8.5_2005Aer (bottom)

scenarios. White areas over the continent denote regions where the signal does not emerge over the 21st century.

Figure 7. Changes in AER between 1860-1890 and 1976-2006 in the soil moisture (a) moisture flux into the region (b), total cloud fraction (c), surface absorption of shortwave radiation (d), 850hPa winds and geopotential height (e; vectors and color contours, respectively). Contour lines in (e) show the climatological 850hPa geopotential height for 1860-1890.

Figure 8. Changes in GHG between 1860-1890 and 1976-2006 in the soil moisture content (a) moisture flux into the region (b), total cloud fraction (c), surface absorption of shortwave radiation (d), 850hPa winds and geopotential height (e; vectors and color contours, respectively). Contour lines in (e) show the climatological 850hPa geopotential height for 1860-1890.

Figures

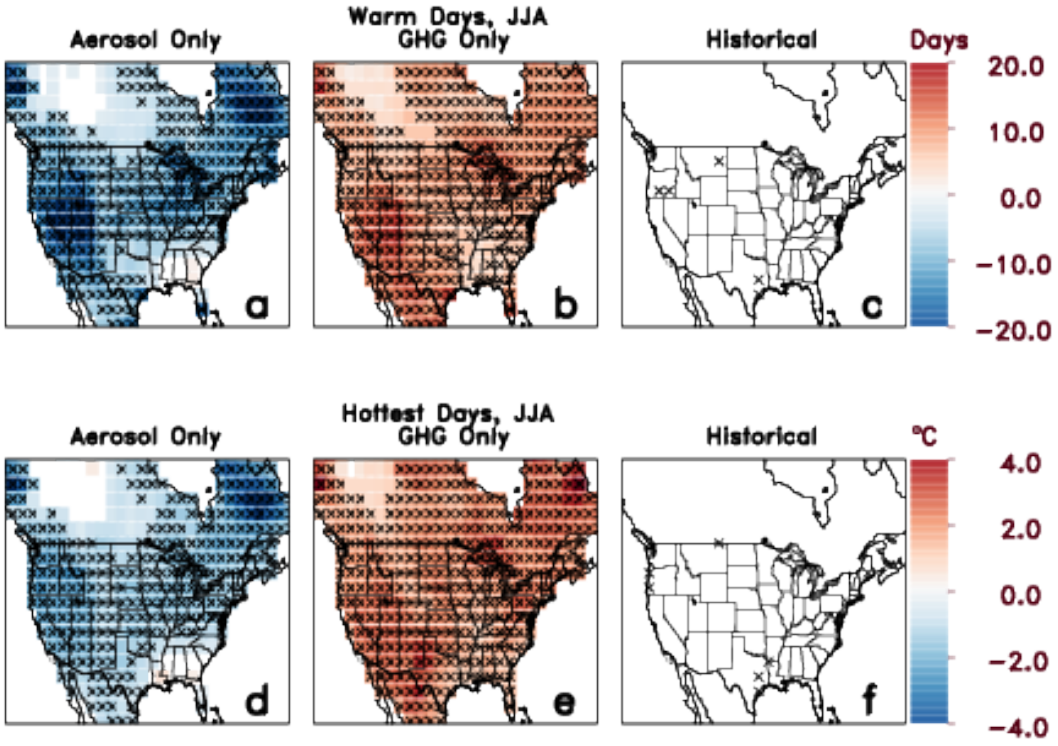

Figure 1. Changes in the 30-year ensemble mean values of summer (JJA) TX90p (top) and TXx (bottom) between the beginning (1860-1890) and end (1976-2006) of the aerosol-only (a), greenhouse gas only (b), and historical simulations (c). Xs denote that the changes are outside of the range of natural variability (95% confidence), as determined from the model's pre-Industrial control simulation.

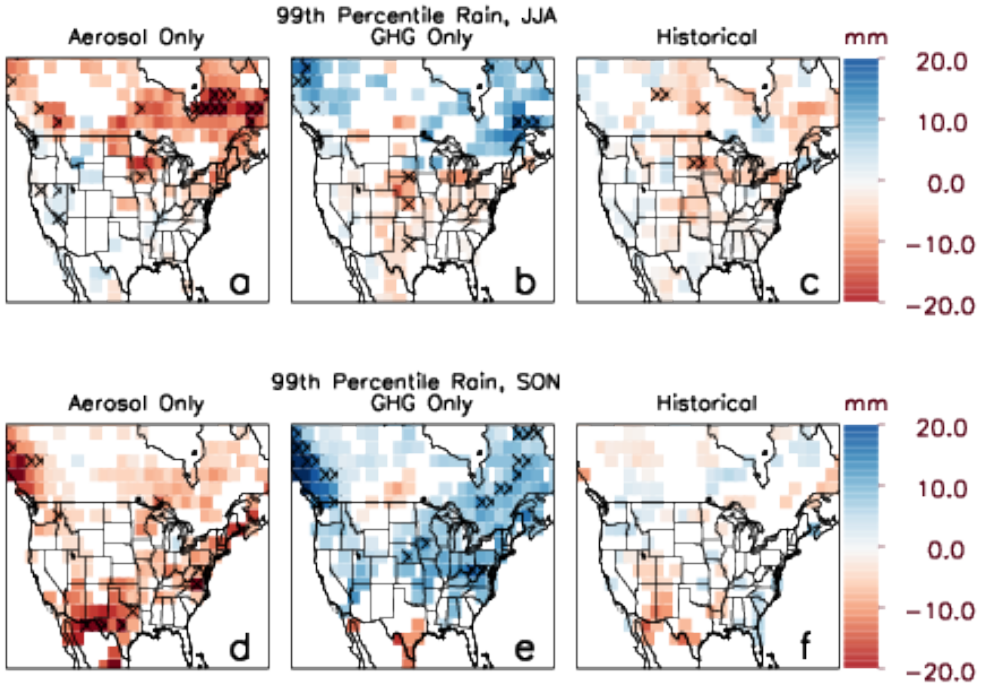

Figure 2. Changes in the 30-year ensemble mean values of R99p between the beginning (1860-1890) and end (1976-2006) of the aerosol only (left), greenhouse gas only (middle) and historical (right) scenarios in winter (top) and spring (bottom).

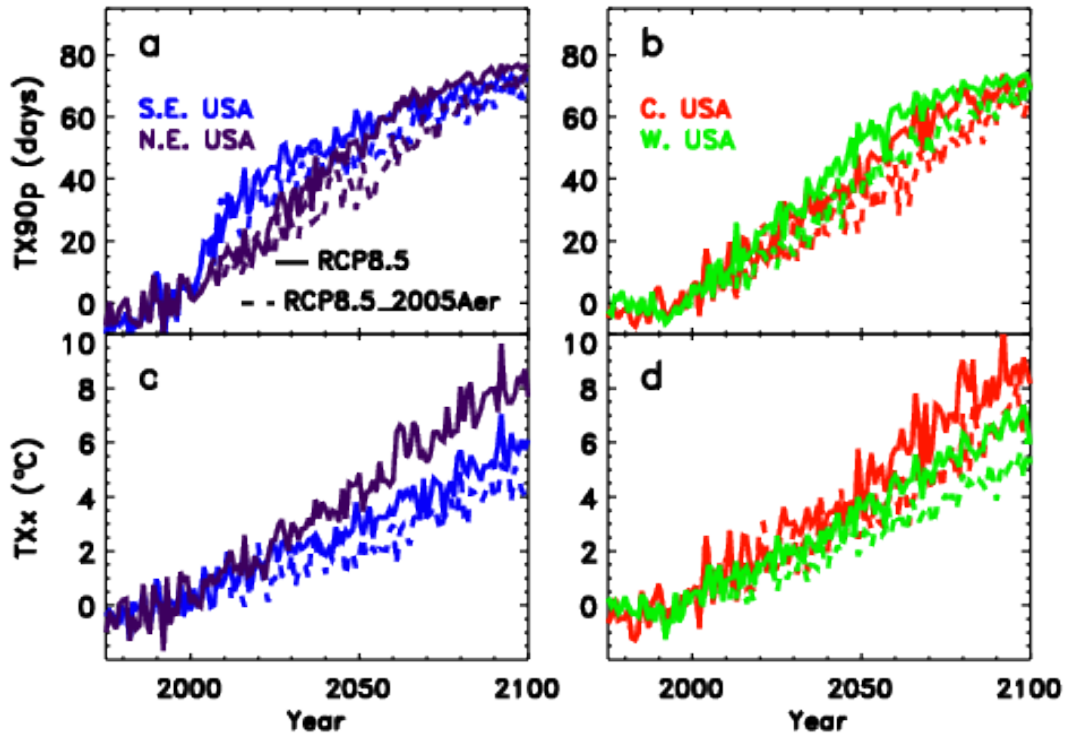

Figure 3. Summertime TX90p (top) and TXx (bottom) for RCP8.5 (solid) and RCP8.5_2005Aer(dashed) for different regions in the U.S., expressed as anomalies with respect to 1975-2005. The tapering off in TX90p at the end of the 21st century is an artifact of the index becoming saturated with respect to the 1961-1990 thresholds.

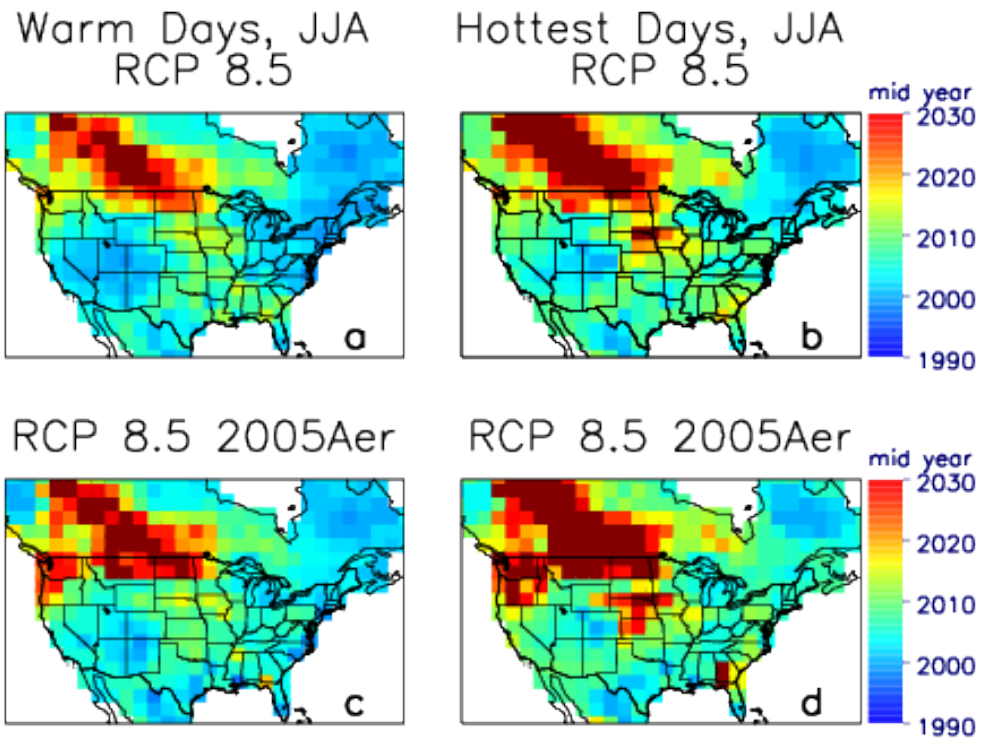

Figure 4. Time of emergence for changes in 30-yr mean TX90p (a)(c) and TXx (b)(d) relative to the present day (1975-2005) for the RCP8.5 scenario (top) and RCP8.5 with aerosols held constant at 2005 levels (bottom). Colors indicate the midpoint of the earliest 30-yr period for which the difference is outside the range of natural variability relative to the pre-Industrial control run.

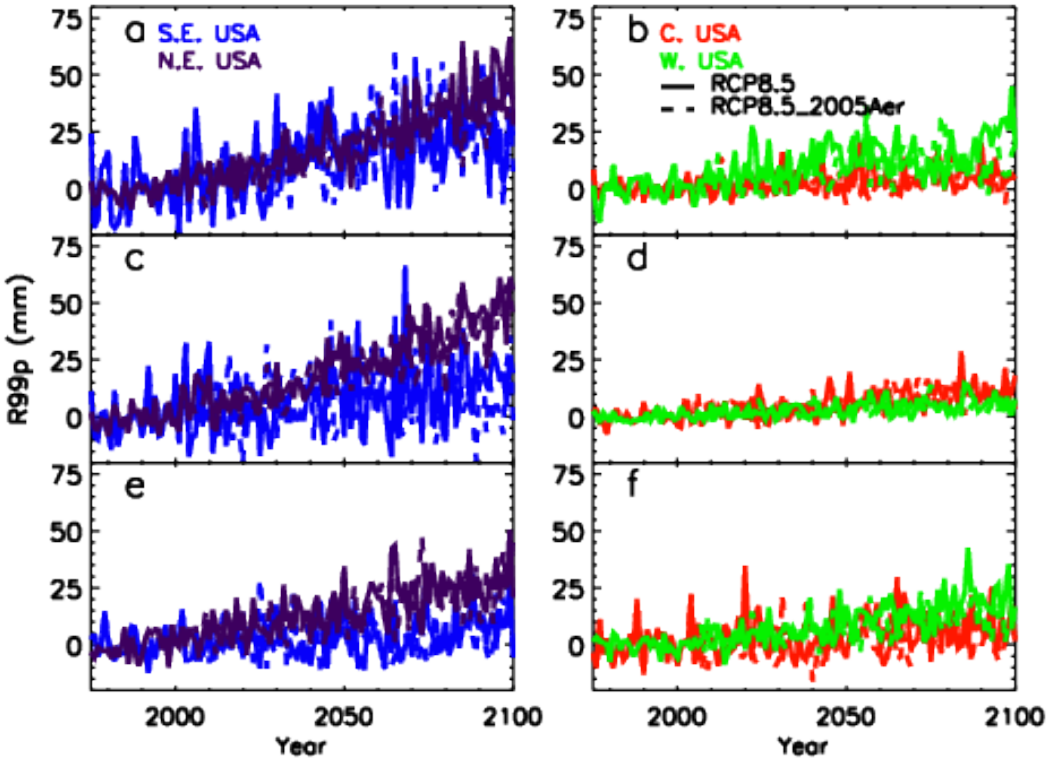

Figure 5. Winter (top), spring (middle), and fall (bottom) R99p for RCP8.5 (solid) and RCP8.5_2005Aer(dashed) for different regions in the U.S., expressed as anomalies with respect to 1975-2005.

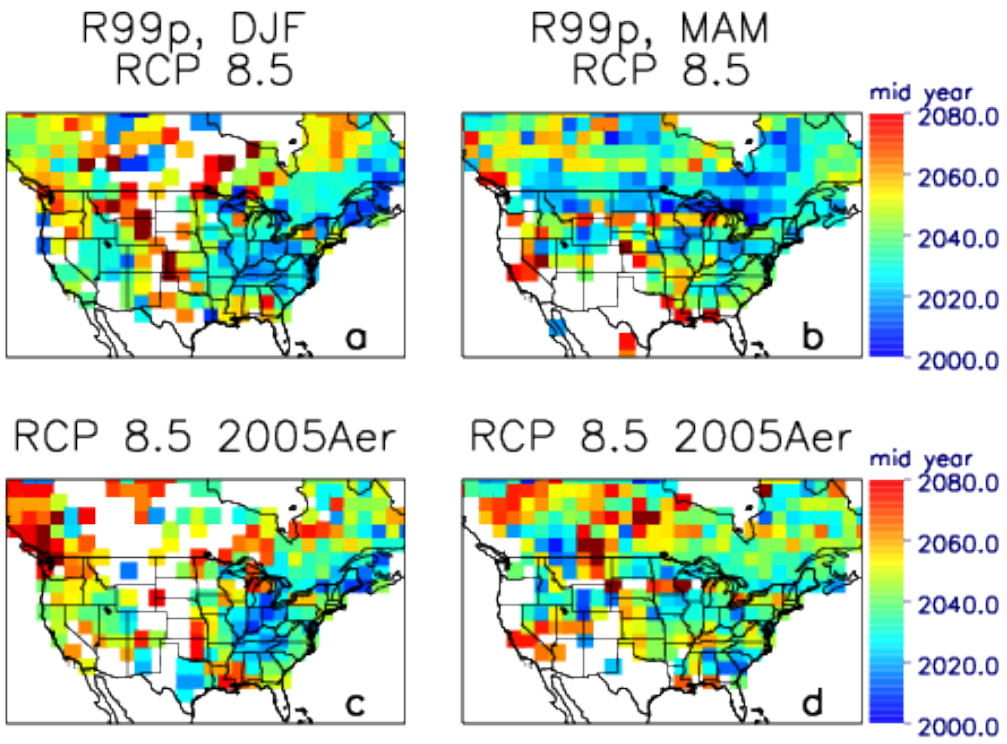

Figure 6. Time of emergence for changes in 30-yr mean R99p for winter (left) and spring (right) relative to the present day (1975-2005) for the RCP8.5 (top) and RCP8.5_2005Aer (bottom) scenarios. White areas over the continent denote regions where the signal does not emerge over the 21st century.

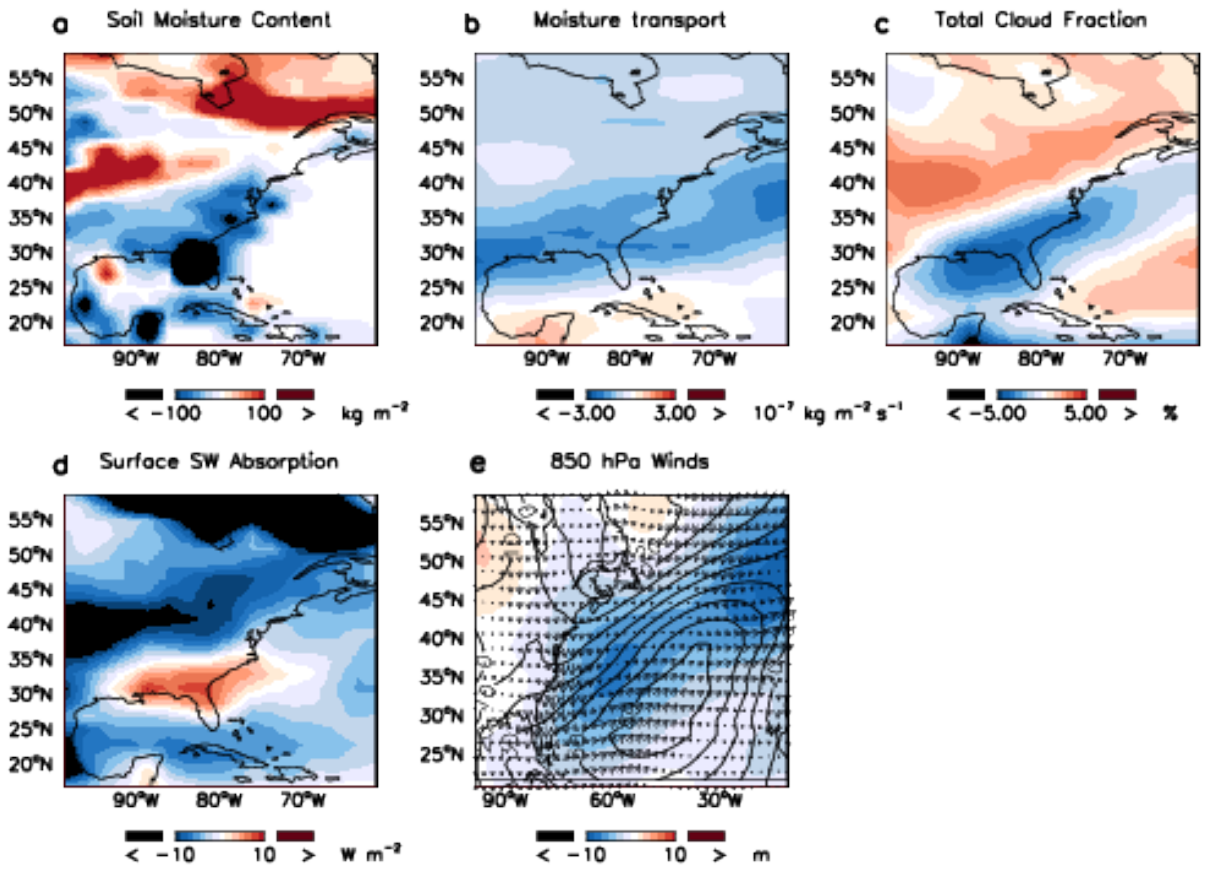

Figure 7. Changes in AER between 1860-1890 and 1976-2006 in the soil moisture (a) moisture flux into the region (b), total cloud fraction (c), surface absorption of shortwave radiation (d), 850hPa winds and geopotential height (e; vectors and color contours, respectively). Contour lines in (e) show the climatological 850hPa geopotential height for 1860-1890.

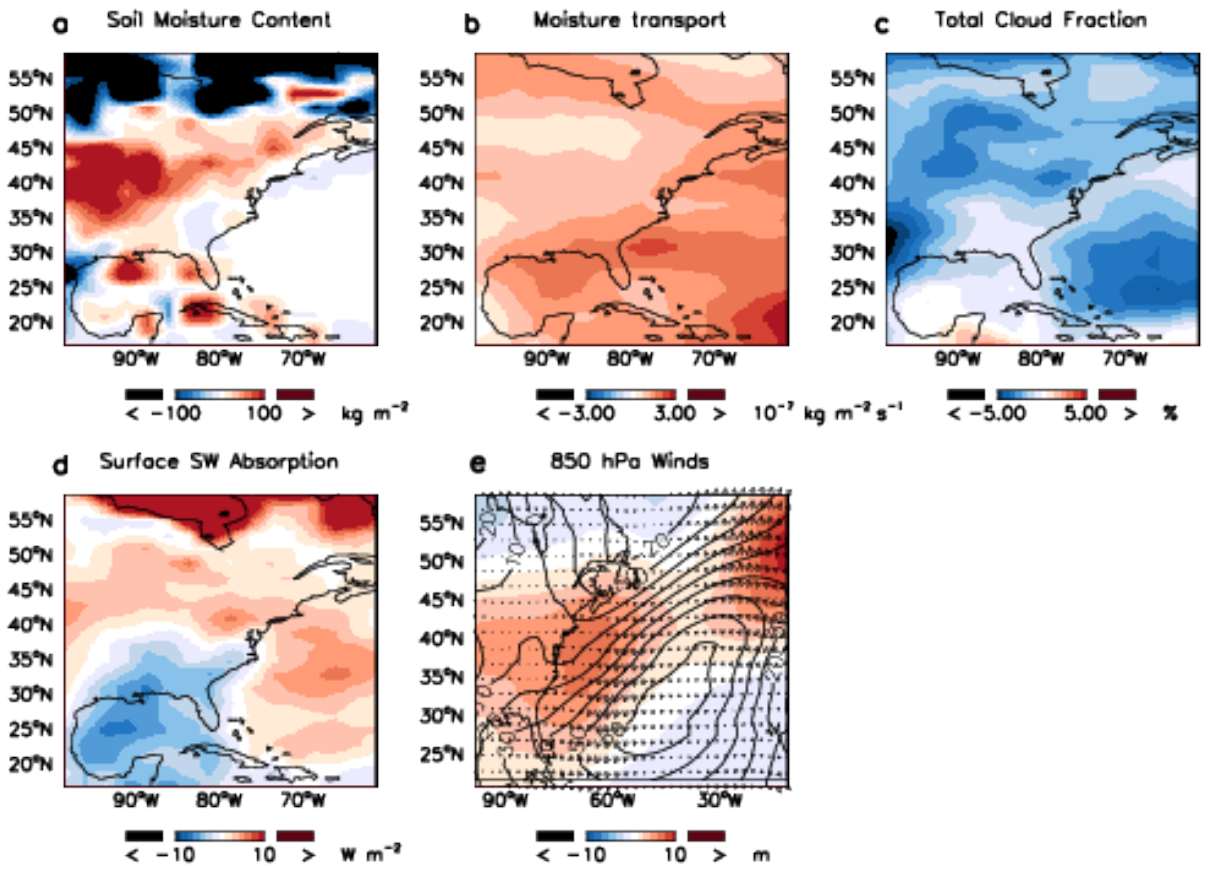

Figure 8. Changes in GHG between 1860-1890 and 1976-2006 in the soil moisture content (a) moisture flux into the region (b), total cloud fraction (c), surface absorption of shortwave radiation (d), 850hPa winds and geopotential height (e; vectors and color contours, respectively). Contour lines in (e) show the climatological 850hPa geopotential height for 1860-1890.